HEAT PIPES AND THROUGH-FLOWS IN GEOTHERMAL RESERVOIRS

M.J. MCGUINNESS

Department of Mathematics, Victoria University of Wellington
Wellington, NZ

SUMMARY— Previous work on steady vertical steam-liquid counterflow in a porous medium, driven by both gravity and capillary pressure, is extended to cases where there is some net mass through-flow. Visualisations of nullcline surfaces are used to analyse solution behaviour. Implications for steady-states with through-flow in geothermal reservoirs are discussed. In particular, a fixed point in the temperature-saturation phase plane is found, when net mass and energy both flow downwards. This fixed point, which dominates solution behaviour, corresponds to a steady solution with constant temperature, pressure and saturation, in free-fall (driven only by gravity).

1. INTRODUCTION

The steady counterflow of steam and liquid in geothermal reservoirs has been the subject of a number of recent studies (McGuinness, 1987, 1988, 1990, 1996a,b; McGuinness *et al.*, 1993; Pruess, 1985; Schubert and Straus, 1979; Straus and Schubert, 1981; Satik *et al.*, 1991). When the mass flows of liquid and steam are roughly equal and in opposite directions, the term ***heatpipe*** is used to describe the flow. This allows efficient heat flow with little or no net mass flow (Martin *et al.*, 1976; Udell, 1985; Pruess, 1985).

The heat pipe is an important part of a model of the Geysers in the seminal paper by White *et al.*, (1971) on vapor-dominated systems. Straus and Schubert (1981) also study heat pipes and have presented case studies of The Geysers and Kawah Kamojang in West Java.

Recent studies (McGuinness *et al.*,, 1993; McGuinness, 1996a,b) have shown the importance of including capillary effects in gravity-driven heat pipes, combining in some degree the engineering and the geothermal approaches, to resolve outstanding questions about steady solution selection in geothermal reservoirs. Net mass flux was taken to be zero.

The effect of changing the steady heat flux has been studied by making heat flux a third dimension, with temperature and saturation being the other dimensions. Nullclines for saturation changes have been viewed as surfaces in this 3D space, and the way that these nullclines move as permeability is reduced has led to an understanding of how conduction affects steady solution behaviour as it becomes more and more dominant.

This work is here extended to explore the effects of allowing a net mass flux through the reservoir. The approach used is to observe changes in nullclines as the net mass flux is varied. It is necessary to view both a saturation nullcline and a temperature nullcline, since temperature reversals become possible with downflows. A short video has been made, showing computer animations of the movement of the nullcline surfaces. This is used in the oral presentation to illustrate some of the points made here.

2. GOVERNING STEADY STATE EQUATIONS

Flow of steam and liquid is vertical and steady, through a 1D homogeneous porous medium with constant properties everywhere. The spatial variable is the elevation z, so that positive flows are upwards. Nomenclature is given in section 8.

Mass and energy conservation yield

$$u_l + u_v = Q_m, \tag{1}$$

$$u_v h_v + u_l h_l = Q + \lambda \frac{\partial T}{\partial z}. \tag{2}$$

Darcy's law gives the momentum balance for the two phases,

$$u_l = -\frac{k k_{rl}}{\nu_l}\left(\frac{\partial P_l}{\partial z} + \rho_l g\right) \tag{3}$$

$$u_v = -\frac{k k_{rv}}{\nu_v}\left(\frac{\partial P_v}{\partial z} + \rho_v g\right). \tag{4}$$

Capillary pressure is taken to be

$$P_c(S,T) = P_v - P_l, \tag{5}$$

and the particular form for P_c is kept general at this point. Vapor-pressure lowering (the Kelvin effect) is also represented in a general way as (after Edlefsen and Anderson, 1948)

$$P_v = f_{vpl}(T,S)\, P_{sat}(T) \tag{6}$$

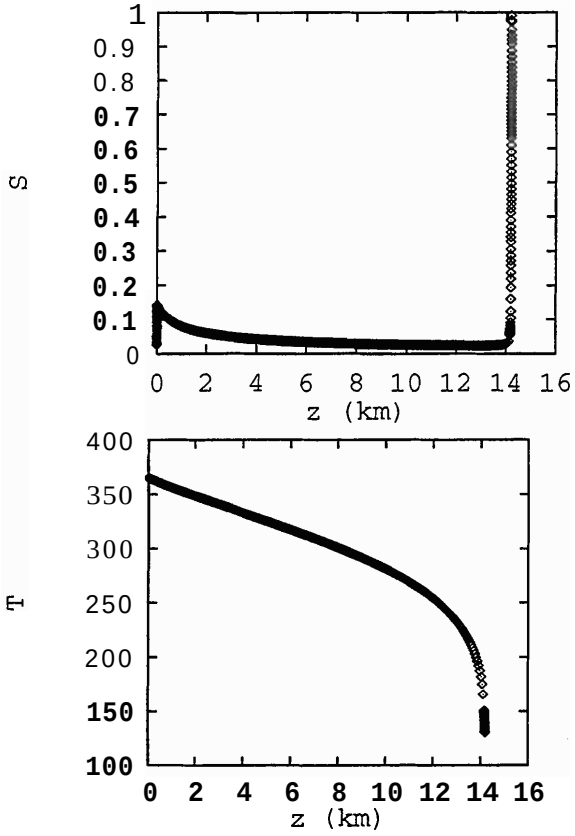

Figure 1. Steady solutions, against z.

where the vapor-pressure lowering factor is approximated by

$$f_{\mathrm{vpl}} = \exp\left\{\frac{m_l P_c(S,T)}{\rho_l \mathrm{R}(T+273.15)}\right\}, \tag{7}$$

and where P_{sat} is the saturated vapor pressure of bulk liquid, obeying the Clausius-Clapeyron relation

$$\frac{dP_{\mathrm{sat}}}{dT} = \frac{\rho_l \rho_v h_{vl}}{(T+273.15)(\rho_l - \rho_v)}. \tag{8}$$

See also Schubert and Straus (1979), McKibbin and Pruess (1989) and Martin et *al.*, (1976) for these. P_v and S are chosen here as the dependent thermodynamic variables. Often in the following, T will be used in place of P_v for illustration purposes.

The conservation equations (1) may be rearranged to obtain

$$\frac{\partial P_v}{\partial z} = -\frac{\mathcal{H}(P_v,S)}{\mathcal{F}(P_v,S)}, \tag{9}$$

$$\frac{\partial S}{\partial z} = \frac{\mathcal{G}(P_v,S)}{\mathcal{F}(P_v,S)}. \tag{10}$$

These form two coupled autonomous first-order ordinary differential equations for P_v and S. The right-hand sides are complicated nonlinear functions of the dependent variables, with no explicit dependence on z. They are given in the appendix. Key parameters affecting the right-hand sides are the heat flux, net mass flux and permeability.

3. SOLUTIONS IN THE PHASE PLANE

Solutions to these two equations depend on the boundary conditions imposed. A natural choice is to specify vapour pressure and saturation at some depth, forming an initial value problem. This corresponds in a fully time-dependent reservoir model to having a constant pressure (or temperature) and saturation at one end, say by connection to a groundwater system, and to having mass and energy flux specified at the other end, leading to the terms Q and Q_m on the right-hand sides of equations (1) and (2).

Each different choice of initial values gives a different solution, which might be plotted as temperature versus z and saturation versus z, as in Fig. 1. These solutions were obtained by solving equations (9) and (10) numerically, with $k = 1\mathrm{d}$, $\mathrm{Q} = 2\mathrm{kW/(d\,m^2)}$, and $Q_m = 0$. In this paper, for illustration purposes, we take $\lambda = 2\mathrm{W/m/K}$, we use linear relative permeability functions with zero residual saturations and we use the Leverett J-function approximation for capillary pressure (Leverett, 1941),

$$P_c = \frac{\sigma(T)J(S)}{\sqrt{k}} \tag{11}$$

However, it is difficult to gain any wide understanding of how solutions behave in general, by simply producing many plots like Fig. 1. Many solutions, corresponding to many different choices of initial values, may be viewed at once by using the phase plane. Vapour pressure or temperature is plotted against saturation, and dependence on z is hidden, although arrows might be used to indicate increasing z. The resulting curves are called trajectories, and an example is shown in Fig. 2, for the same parameter values as in Fig. 1. The smooth closed curve is the $\mathcal{G} = 0$ nullcline. Arrows point in the direction of increasing z.

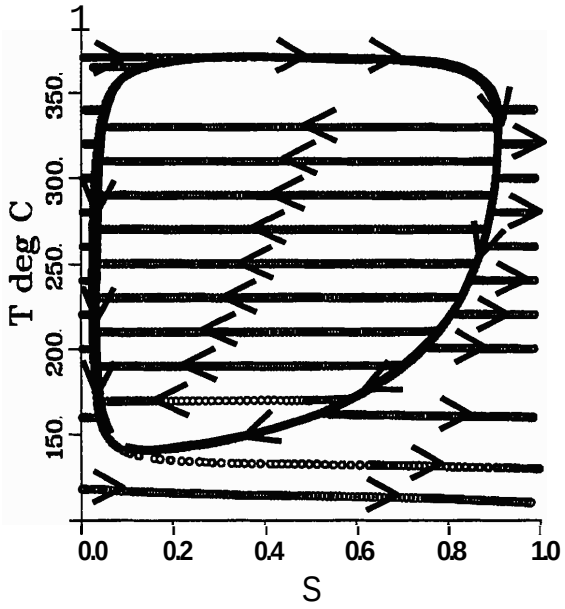

Figure 2. Steady solutions, in the phase plane.

In the usual theory of the phase plane, the first feature that is looked for is fixed points, where the right-hand sides of the two differential equations are simultaneously zero. Fixed points control trajectory behaviour, locally

and globally, particularly in the absence of periodic solutions. Note that in the usual geothermal situation, temperature or pressure increase monotonically with depth, so that the phase plane plots look similar to saturation versus depth plots, and there are no places where $\mathcal{H} = 0$. It can be shown from the form of $\mathcal{H}$ that it is never zero when Q is positive. Hence there are no fixed points or periodic solutions when Q is positive.

4. NULLCLINES

In the absence of fixed points, another useful characteristic of solutions is the nullcline, where one right-hand side is zero. In our case, this is $\mathcal{G} = 0$, where saturation reverses direction. The heavy curve in Fig. 2 can be used to abstract solution behaviour, and it is possible to infer qualitative solution behaviour knowing only the nullcline.

Changing the steady heat flux changes the nullcline. Fig. 3 shows many nullclines, one for each of many values of heat flow Q, on the same phase plane. Other parameter values are as for Fig. 1.

A natural way to view the nullclines is as level curves of a nullcline surface, obtained by plotting $\mathcal{G} = 0$ as a surface in a 3D space, with coordinates the phase plane and Q. The way that nullcline surfaces move as permeability is varied is explored in McGuinness (1996a,b).

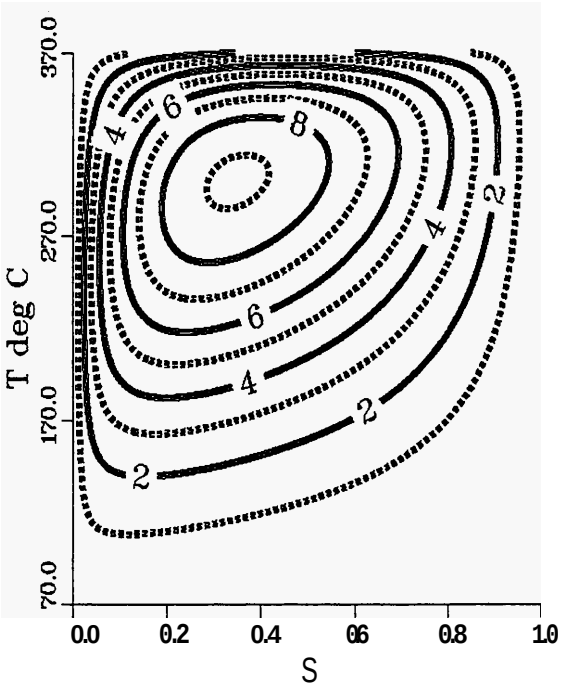

Figure 3. $\mathcal{G} = 0$ nullclines, as labelled for various values of heat flow Q (kW/m^2).

5. VARYING NET MASS FLUX

In a two-phase geothermal reservoir, there is often a net mass throughflow, and it may even be a downflow in some areas. When a downflow of heat is allowed, it is also possible that $\mathcal{H} = 0$. Then there are two nullcline surfaces, one for saturation reversals and one for temperature reversals. These have been obtained by numerically evaluating the right-hand sides of equations (9) and (10) for a range of values of S, P_v, Q, and putting a surface through zero values of $\mathcal{G}$ and $\mathcal{H}$.

Visualisations of these surfaces are shown in Fig. 4 for both positive and negative values of net mass flux, when permeability is 0.1 md. This figure is at the end of this paper. The surface shown as a wire frame is the saturation nullcline, and the temperature nullcline surface is shown as a solid. Two views of each mass flux are shown.

For positive net mass fluxes, as net mass upflow increases, both surfaces move upwards. They do not cross each other. The saturation nullcline surface moves upwards faster at the high temperature end and at the low liquid saturation end. This is due to the higher enthalpy of a high temperature mixture, and of steam.

Visualisations of the nullcline surfaces for negative net mass fluxes reveal a new and significant phenomenon — the surfaces cross each other. This corresponds in the phase plane to there being a fixed point. that is, there is a steady solution with constant temperature and saturation everywhere. This solution corresponds to free-falling steam and liquid, such that

$$Q_m = u_v + u_l = -gk\left(\frac{k_{rl}\rho_l}{\nu_l} + \frac{k_{rv}\rho_v}{\nu_v}\right), \qquad (12)$$

$$Q = u_v h_v + u_l h_l = -gk\left(\frac{k_{rl}\rho_l h_l}{\nu_l} + \frac{k_{rv}\rho_v h_v}{\nu_v}\right). \qquad (13)$$

That is,

$$Q_m = -gk\frac{\rho}{\nu}, \qquad (14)$$

$$Q = -gk\frac{\rho h}{\nu}, \qquad (15)$$

where ρ, h and ν are two-phase flowing densities, defined by the above equations in terms of the kinematic viscosity rather that the usual dynamic viscosity (see, e.g., Weir, 1994).

The accessible values of heat and mass flux can be calculated, by evaluating the right-hand sides for various values of pressure and saturation. The results of this are plotted in Fig. 5 as heat flow Q against net mass flux Q_m, with the signs reversed for convenience. The straight line corresponds to the expected relationship if the two-phase fluid had the enthalpy of pure steam at 100°C. The line corresponding to pure liquid lies very close to the Q_m axis on this scale. The region of possible heat and mass fluxes is bounded by pure steam and pure liquid lines, and is generally smaller. All values of temperature and saturation are possible.

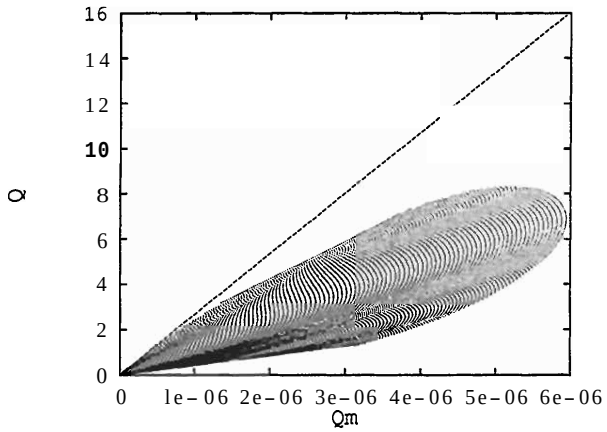

Figure 5. Possible values of heat flux Q (W/m^2) and net mass flux (kg/s/m^2), when at the fixed point. Both fluxes are negative — the negative sign has been dropped.

In the study of systems of differential equations, the stability of a fixed point is of interest, as it governs local trajectory behaviour. Examination of the nullclines reveals that the fixed point is a node, stable when integrating in the positive z direction, which is upwards. Fig. 6 confirms this with trajectories calculated numerically for $Q_m = -10^{-6}$kg/m^2/s, $Q = -1$W/m^2, and $k = 0.1$md. Arrows show the direction of increasing z, or upwards movement. Note the trajectories converging to the fixed point, indicated by the circle at 228°C and S = 0.17. When temperature is high enough, there are trajectories that simply move across the top of the plot, without being attracted to the fixed point.

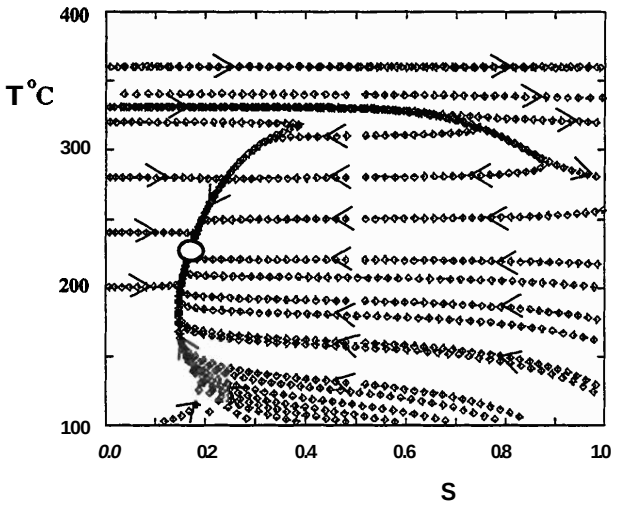

Figure 6. Trajectories in the temperature-saturation phase plane, when mass and heat fluxes are negative, and there is a fixed point.

6 CONCLUSIONS

The main result of this paper is that, in contrast to the cases with zero net mass fluxes and upwards energy fluxes, a fixed point is observed in the temperature-saturation phase plane, where the temperature and saturation nullclines cross each other. This fixed point is a feature that dominates steady solution behaviour in the phase plane. It only exists for a certain range of mass downflows and heat downflows.

Provided boundary conditions are chosen appropriately, many solutions in the phase plane approach this fixed point, which corresponds to a free-falling mixture of steam and liquid. The steam and liquid fall at different mass flux densities in general, and temperature and saturation are constant everywhere. The length of such solutions is unbounded.

7 ACKNOWLEDGEMENTS

The visualizations that provided valuable assistance with the phase plane studies were performed on a Silicon Graphics Iris Indigo, funded by the Lotteries Science Research Fund, New Zealand, and the Internal Grants Committee of Victoria University of New Zealand. Thanks to Robert McKibbin for fruitful discussions.

8 NOMENCLATURE

h	specific enthalpy (J/kg)
h_{vl}	latent heat of vaporization (J/kg)
J	the Leverett J-function, $1.417(1-S) - 2.12(1-S)^2 + 1.263(1-S)^3$
k	permeability
k_r	relative permeability
md	millidarcy, 10^{-3} darcy, 10^{-15}m^2
m_l	molecular weight of liquid water (kg/kmol)
u	mass flux density (kg s^{-1} m^{-2})
P	pressure (Pa)
P_c	capillary pressure (Pa)
Q	energy flux (W/m^2)
Q_m	net mass flux (kg s^{-1} m^{-2})
R	gas constant (m^3 Pa K^{-1} mol^{-1})
S	liquid saturation
T	temperature (°C)
z	vertical distance (m)

Greek symbols

λ	thermal conductivity (W/m/°C)
λ_l	liquid mobility (kk_{rl}/ν_l)
λ_v	vapor mobility (kk_{rv}/ν_v)
ν	kinematic viscosity (m^2/s)
ρ	specific density (kg/m^3)
σ	surface tension (kg/s^2)

Subscripts

l liquid water
v steam or vapour phase

9 REFERENCES

N.E. Edlefsen, and A.B.C. Anderson (1948) Thermodynamics of Soil Moisture, *Hilgardia,* **15** No.2, 231-298.

M.J. McGuinness (1987), Unstable Heat Pipes, in *the proceedings of the 9th New Zealand Geothermal Workshop,* Auckland University, November 1987, 147–152.

M.J. McGuinness (1988), Heat Pipe Stability and Upstream Differencing, in *the proceedings of the 10th New*

Zealand Geothennul Workshop, Auckland University, November 1988,117–121.

M.J. McGuinness (1990), Heat Pipe Stability in Geothermal Reservoirs, in *theproceedings of the 1990 Geothennul Symposium, GRC, Hawaii,* Part I, 1301-1308 (1990).

M.J. McGuinness (1996a) Steady solution selection and existence in geothermal heat pipes. I: the convective case, *Int.* **J.** *Heat and Mass Transfel;* **39** No. 2, 259–274.

M.J. McGuinness (1996b), Steady solution selection and existence in geothermal heat pipes. II: the conductive case, *Int.* **J.** *Heat and Mass Transfel;* (in press).

M.J. McGuinness, M. Blakeley, K. Pruess, and M.J. O'Sullivan (1993) Geothermal Heat Pipe Stability: Solution Selection by Upstreaming and Boundary Conditions, *Transport in Porous Media* **11**, 71–100.

R. McKibbin, and K. Pruess (1989), Some effects of noncondensiblegas in geothermal reservoirs with steam-water counterflow, *Geothennics,* 18No.3, 367–375 (1989).

M.C. Leverett (1941) Capillary behaviour in porous solids, *AIME Trans.* 142, 52.

J.C. Martin, R.E. Wegner and F.J. Kelsey (1976), One-dimensional convective and conductive geothermal heat flow, *Proc. 2nd Workshop on Geothennul Reservoir Engineering,* Stanford University, pp.251–262.

K. Mess (1985), A quantitative model of vapor-dominated geothermal reservoirs as heat pipes in fractured porous rock, *Trans. Geotherm. Res. Council* **9** II pp.353–361.

C. Satik, M. Parlar, and Y.C. Yortsos (1991), A Study of Steady-state Steam-water Counterflow in Porous Media, *Int.* **J.** *Heat and Mass Transfer,* **34** No.7, 1755–1772.

G. Schubert and J.M. Straus (1979), Steam-water Counterflow in Porous Media, **J.** *Geophys. Res.* **84** 1621–1628.

G. Schubert and J.M. Straus (1981), Gravitational stability of water over steam in vapor-dominated geothermal systems, *J. Geophys. Res.* 85 6505–6512.

J.M. Straus and G. Schubert (1981), One-dimensional model of vapor-dominated geothermal systems, **J.** *Geophys. Res.* 86 9433–9438.

K.S. Udell (1985), Heat Transfer in Porous Media Considering Phase Change and Capillarity — the Heat Pipe Effect, *Int.* **J.** *Heat and Mass Transfer* 28 485–495.

G.J. Weir (1994), The relative importance of convective and conductive effects in two-phase geothermal fields, *Trans. in Porous Media* 16 289–298.

D.E. White, J.P. Muffler, and A.H. Truesdell (171), Vapor-dominated hydrothermal systems compared with hot-water systems, *Economic Geology,* 66 75–97.

10 APPENDIX

The right-hand sides of equations 9 and 10 are

$$\mathcal{F} = \frac{P_0}{H_0}\left[\lambda_l\left(1 - \frac{\partial P_c}{\partial T}\frac{\partial T}{\partial P_v}\right) + \lambda_v\right]\left(\lambda_l h_l - \frac{A\,\partial T}{\frac{\partial P_c}{\partial S}\partial S} + \lambda_l h_l \frac{\frac{\partial P_c}{\partial T}\frac{\partial T}{\partial S}}{\frac{\partial P_c}{\partial S}}\right) \tag{16}$$

$$-\lambda_l\left(1 + \frac{\frac{\partial P_c}{\partial T}\frac{\partial T}{\partial S}}{\frac{\partial P_c}{\partial S}}\right)\left(\lambda_l h_l + \lambda_v h_v - A\,h\,\frac{\partial P_c}{\partial T}\frac{\partial T}{\partial P_v} + \lambda\frac{\partial T}{\partial P_v}\right), \tag{17}$$

$$\mathcal{G} = g\left[\left(\lambda_l\left(1 - \frac{\partial P_c}{\partial P_v}\right) + \lambda_v\right)(Q/g + \lambda_l\rho_l h_l + \lambda_v\rho_v h_v)\right. \tag{18}$$

$$\left. - (\lambda_l\rho_l + \lambda_v\rho_v + Q_m/g)\left(\lambda_l h_l\left(1 - \frac{\partial P_c}{\partial P_v}\right) + h_v\lambda_v + \lambda\frac{\partial T}{\partial P_v}\right)\right], \tag{19}$$

$$\mathcal{H} = -g\left[(Q/g + \lambda_l\rho_l h_l + \lambda_v\rho_v h_v)\lambda_l\left(1 + \frac{\frac{\partial P_c}{\partial T}\frac{\partial T}{\partial S}}{\frac{\partial P_c}{\partial S}}\right)\right. \tag{20}$$

$$\left. - (\lambda_l\rho_l + \lambda_v\rho_v + Q_m/g)\left(\lambda_l h_l\left(1 + \frac{\frac{\partial P_c}{\partial T}\frac{\partial T}{\partial S}}{\frac{\partial P_c}{\partial S}}\right) - \frac{\lambda}{\frac{\partial P_c}{\partial S}}\frac{\partial T}{\partial S}\right)\right], \tag{21}$$

$$\epsilon = \frac{1}{\mathrm{Po}}\frac{\partial P_c}{\partial S}. \tag{22}$$

and where P_v and z have been non-dimensionalizedby dividing by a reference pressure P_0 and a reference depth H_0.

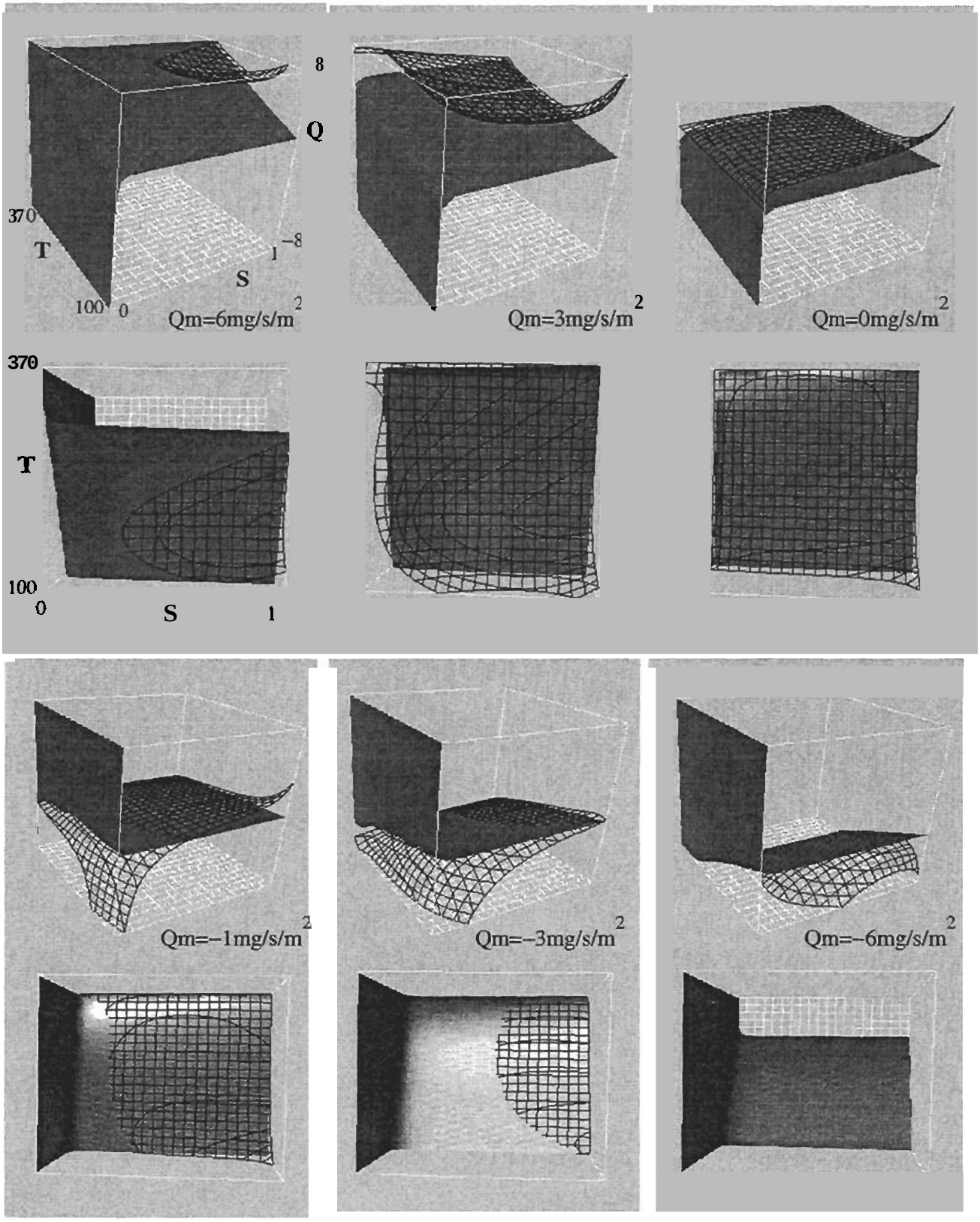

Figure 4. Nullcline visualisations, for permeability 0.1 md, with various net mass fluxes. A side view and a top view is shown of each.